WEP Warwick Evans Publishing

International Journal of Natural Resources and Environmental Studies

ISSN: 3006-2012 (Print), ISSN: 3006-0834 (Online) | Volume 7, Number 3, Year 2025
DOI: https://doi.org/10.62051/ijnres.v7n3.02
Journal homepage: https://wepub.org/index.php/IJNRES/index

Numerical Simulation of Single Tooth Rock Breaking Mechanism Under High Temperature Environment

Xian Ye*, [1], Qingchun Gao[2], Xuan Zhang[3], Shengxu Liu[4]

[1]China National Petroleum Corporation Great Wall Drilling Company Engineering Technology Research Institute, Panjin 124010, China;

[2]Great Wall Drilling Company (GWDC), Beijin 100101, China;

[3]China National Petroleum Corporation Liaohe Oilfield Qingyang Exploration and Development Branch, Qingyang 745100, China;

[4]New Energy Business Department (Power Supply Company) of CNPC Jidong Oilfield, Tangshan 063200, China.

*Corresponding Author: Xian Ye

ABSTRACT

In high-temperature geothermal drilling, due to the high hardness and strong abrasiveness of the formation rock, and the rock drillability is significantly reduced in high-temperature environments, the working efficiency of traditional PDC drill bits decreases, and it is necessary to further explore the rock-breaking mechanism under high-temperature conditions. To this end, the research systematically examined the influence of high temperature on the single-tooth rock breaking process. Through numerical simulation, the effect of temperature on the single-tooth cutting process was explored. The results show that as the temperature increases, the rock damage first decreases and then increases. The damage is minimal at 200°C. The weakened rock strength at high temperature helps to improve the rock breaking efficiency. The Cpress stress of the tooth edge increases from the lowest point on both sides and is symmetrically distributed. The contact area is about 50°. The stress is the highest and fluctuates the most at 200°C, which is easy to cause uneven wear and is not conducive to the life of the cutting teeth. If the temperature continues to increase, the stress distribution will tend to Uniform; the increase in rake angle leads to the expansion of the high-temperature zone on the tooth surface, intensification of stress and fluctuations, and aggravates unbalanced wear; the increase in penetration increases the Cpress stress, expands the contact area, and intensifies stress fluctuations, which also affects the life of the cutting teeth. Tooth profile comparison shows that 3D tooth profiles such as roof teeth and Mercedes-Benz teeth have the advantages of large rock damage, high rock breaking efficiency, and small stress fluctuations in high-temperature and high-abrasive formations, and are more suitable for high-temperature geothermal drilling. The research results provide key theoretical support and parameter basis for the optimal design of high-temperature geothermal drill bits.

KEYWORDS

High temperature geothermal well; PDC bit; Rock breaking mechanism; Numerical simulation.

1. INTRODUCTION

As a renewable and clean energy source, geothermal energy has gained increasing global attention. With the continuous exploitation of oil and coal, non-renewable resources are dwindling[1,2], and geothermal energy has become an effective alternative. The utilization efficiency of geothermal energy is expected to reach 30%–80% of global energy demand, and its applications are expanding[3-

6]. In low- to medium-temperature formations, the challenges faced by drill bits are relatively minor. However, in high-temperature formations, the performance of drill bits significantly decreases due to changes in the downhole environment.

High-temperature geothermal drilling often encounters hard and highly abrasive metamorphic or igneous rocks[7]. Under high temperatures, the difficulty of drilling increases significantly, and downhole uncertainties are numerous[8]. Even PDC bits, which perform well in oil and gas drilling, show significantly reduced performance in high-temperature geothermal drilling[9],[10]. Currently, roller cone bits are mainly used in geothermal drilling. Tungsten carbide insert roller cone bits can withstand temperatures up to 150°C. Beyond this temperature, the rubber in the bit bearing ages, and the lubricant fails prematurely, allowing drilling fluid or rock cuttings to enter the bearing and accelerate its damage. Additionally, high temperatures significantly weaken the strength of the teeth, leading to tooth loss or breakage, severely shortening the service life of roller cone bits.

In recent years, with the rapid development of PDC bits, their high rock-breaking efficiency and strong penetration ability have led to widespread application. Over 90% of global drilling footage is now completed by PDC bits[12]-[14]. The rock temperature in high-temperature geothermal wells generally ranges from 150–650°C, far exceeding that of conventional oil and gas drilling. At these temperatures, the mechanical properties of rock change significantly compared to ambient conditions, and high temperature has become a key factor limiting bit performance. Conventional PDC bits often fail before drilling to a certain depth in high-temperature geothermal wells and show no clear advantage over roller cone bits.

Currently, there is a lack of technology for high-temperature PDC drill bits designed specifically for geothermal drilling in the country. The few existing geothermal drill bit products are mostly roller cone bits, and their applications are limited to relatively shallow depths. PDC bits have not yet been widely accepted in the geothermal drilling industry, with the general belief that roller cone bits are more suitable for such formations. The main reasons are: (1) severe thermal wear of cutting teeth in high-temperature geothermal drilling, leading to significantly reduced bit performance and service life; and (2) the lower economic return of geothermal drilling compared to oil and gas drilling, with PDC bits being significantly more expensive than roller cone bits.

2. ROCK MATERIAL CONSTITUTIVE MODEL

For the plastic constitutive relationship of rock materials, this paper adopts the Drucker–Prager strength criterion, which is suitable for granular materials. This criterion considers the influence of intermediate principal stress on failure characteristics and reflects the dilatancy effect caused by yielding. It is widely used in rock-breaking simulations. The D–P criterion is expressed using the normal and shear stresses on the Regular octahedron[15, 16]:

$$\tau_{oct} = \tau_0 + m\sigma_{oct} \tag{1-1}$$

$$\begin{cases} \tau_{oct} = \dfrac{1}{3}\sqrt{(\sigma_1-\sigma_2)^2+(\sigma_2-\sigma_3)^2+(\sigma_3-\sigma_1)^2} \\ \sigma_{oct} = \dfrac{1}{3}(\sigma_1+\sigma_2+\sigma_3) \\ m = -\sqrt{6}\alpha, \quad \tau_0 = \dfrac{\sqrt{6}}{3}k \end{cases} \tag{1-2}$$

$$\alpha = \frac{2\sin\varphi}{\sqrt{3}(3-\sin\varphi)} \tag{1-3}$$

$$k = \frac{6c\cos\varphi}{\sqrt{3}(3-\sin\varphi)} \tag{1-4}$$

In the above equation: σ_1, σ_2, and σ_3 are the principal stresses of the rock, while k and α are parameters related to the rock's cohesion and the internal friction angle (φ). During the cutting process, rocks undergo shear failure[17]. Therefore, for rock materials that follow the Drucker-Prager criterion, a shear damage model is chosen as the damage criterion for rocks. The shear damage criterion serves as the initiation criterion for rock failure. It is assumed that the equivalent plastic strain in the initial failure state is a function related to shear stress rate (θ_s) and plastic strain rate ($\bar{\varepsilon}^{\&pl}$), represented by variables $\bar{\varepsilon}_f^{pl}$ and $\bar{\varepsilon}_f^{pl}(\theta_s,\bar{\varepsilon}^{\&pl})$.

$$\theta_S = (q + k_S p)/\tau_{\max} \tag{1-5}$$

In the above equation: τ_{max} is the maximum shear stress of the rock; k_s is a parameter related to the rock material; p is the equivalent compressive stress of the rock; q is the MISES equivalent stress of the rock.

$$p = -\frac{1}{3}trace(\sigma) = -\frac{1}{3}(\sigma_3 + 2\sigma_1) \tag{1-6}$$

$$q = \sqrt{\frac{1}{2}[(\sigma_1-\sigma_2)^2 + (\sigma_2-\sigma_3)^2 + (\sigma_3-\sigma_1)^2]} = \sigma_1 - \sigma_3 \tag{1-7}$$

The failure of rock during the cutting process is a continuous process, not a single state. Fig. 1 shows the stress–strain curve of the material during damage. The solid line represents the stress–strain relationship after the material has been damaged, while the dashed line represents the relationship without damage. The response after damage is related to the size of the element.

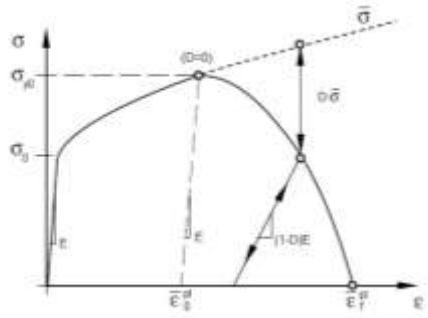

Fig. 1 Stress-strain relationship curve after rock damage

In the figure, σ_{y0} is the yield stress at damage initiation, $\bar{\varepsilon}_0^{pl}$ is the equivalent plastic strain at damage initiation, $\bar{\varepsilon}_f^{pl}$equivalent plastic strain at failure, also called equivalent fracture plastic strain.

In the finite-element model, a characteristic length L_s linked to the integration point is required to apply the stress–displacement concept.The energy needed to open a unit area of crack is then given by

$$G_f = \int_{\bar{\varepsilon}_0^{pl}}^{\bar{\varepsilon}_f^{pl}} L_s \sigma_y \dot{\bar{\varepsilon}}_f^{pl} = \int_0^{\bar{u}_f^{pl}} \sigma_y \dot{\bar{u}}_f^{pl} \tag{1-8}$$

In the equation, the fracture work (work per unit crack area) defines the equivalent fracture plastic displacement $\bar{u}_f^{pl}$, and this work is conjugate to the yield stress after damage initiation.Before damage initiation: $\dot{\bar{u}}_f^{pl} = 0$

After damage initiation:

$$\dot{\bar{u}}_f^{pl} = L\dot{\bar{\varepsilon}}_f^{pl} \tag{1-9}$$

The geometric shape of the element determines the definition of the characteristic length: for solid elements, it is generally expressed by the cube root of the volume of the integral point element, that is:

$$L_s = \sqrt[3]{L_{s1} \times L_{s2} \times L_{s3}} \tag{1-10}$$

In the equation, L_{s1}, L_{s2}, and L_{s3} are the lengths of the element edges.

3. FINITE ELEMENT MODEL ESTABLISHMENT

In order to facilitate calculation and analysis, the following assumptions are made for the interaction model between cutting teeth and rocks:

Rock is a homogeneous, continuous, and isotropic medium;

Failed rock elements are removed from the model, and their influence on subsequent drilling is ignored;

The cutting tooth is much harder and stronger than the rock and does not wear during cutting;

Heat transfer between the tooth and rock is mainly through conduction,and the effects of convection heat transfer and thermal radiation are ignored.

Selected test results of granite and sandstone at different temperatures are shown in Tables 1 and 2.

Table. 1 Partial rock mechanical properties of granite

Temperature(℃)	25	100	200	300	400	500
Compressive strength (MPa)	133.33	146.89	157.81	86.29	76.52	75.83
elastic modulus (GPa)	5.798	7.764	8.649	4.4	4.225	4.156
Shear strength (MPa)	15.92	17.35	20.85	14.64	14.23	13.96
Poisson's ratio	0.206	0.175	0.154	0.152	0.147	0.149
internal friction angle (°)	20.7	21.1	28.5	18.7	16.5	16.2

Table. 2 Some rock mechanical properties of sandstone

Temperature(℃)	25	100	200	300	400	500
Compressive strength (MPa)	61.64	59.13	56.56	46.03	40.21	39.86
elastic modulus (GPa)	3.999	4.104	4.395	4.487	4.533	4.486
Shear strength (MPa)	14.61	12.23	11.62	10.32	9.52	9.35
Poisson's ratio	0.143	0.125	0.117	0.108	0.082	0.081
internal friction angle (°)	36.95	35.51	31.72	30.55	28.75	28.34

The rock mechanics curves of granite and sandstone at high temperatures are shown in Fig. 2 and Fig**. 3**. It can be seen from the figure that as the temperature increases, the compressive strength, shear strength, elastic modulus, and internal friction angle of granite first increase and then decrease, and the mechanical property parameters are maximum when the temperature is about 200°C; as the temperature increases, the compressive strength, shear strength, and internal friction angle of sandstone gradually decrease. When the temperature reaches a certain value, the rock mechanical

properties are greatly reduced, that is, the rock mechanical properties are more sensitive to temperature changes.

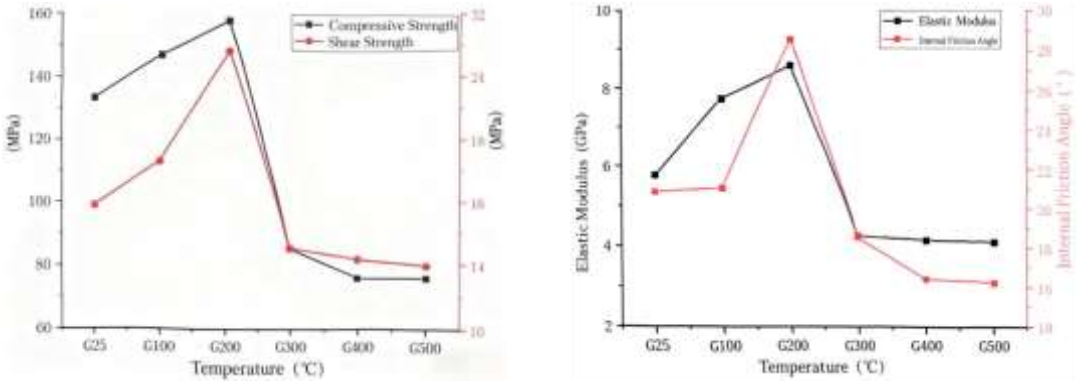

(a) Compressive strength and shear strength (b) Elastic modulus and internal friction angle

Fig. 2 Relationship curves of mechanical properties of granite at different temperatures

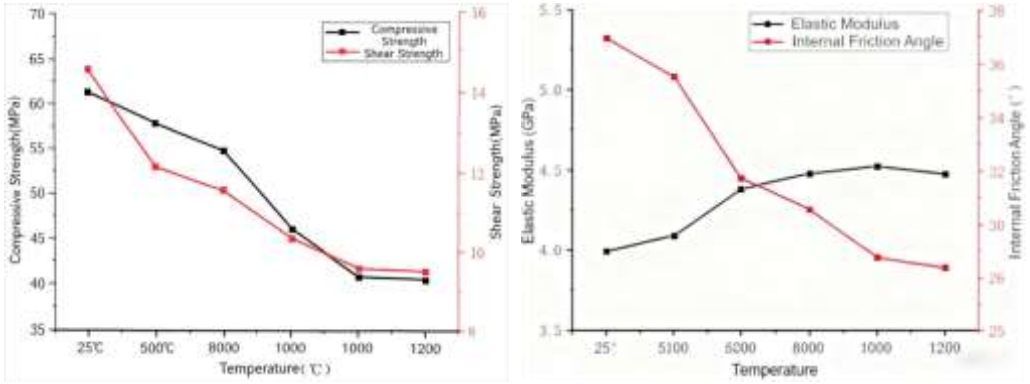

(a) Compressive strength and shear strength (b) Elastic modulus and internal friction angle

Fig. 3 Relationship curves of sandstone mechanical properties at different temperatures

The finite element model for single-tooth cutting is shown in Fig. 4The rock dimensions are 100 mm × 80 mm × 40 mm; the cutter diameter is 15.875 mm, thickness 8 mm, and the PDC layer thickness 2 mm. The rake angle is 15°, and the back rake angle is 0°. The model uses C3D8RT elements with local mesh refinement. The cutting speed is 0.3 m/s, and simulations are conducted at 100°C, 200°C, 300°C, 400°C, and 500°C using ABAQUS/Explicit coupled temperature-displacement dynamic analysis.

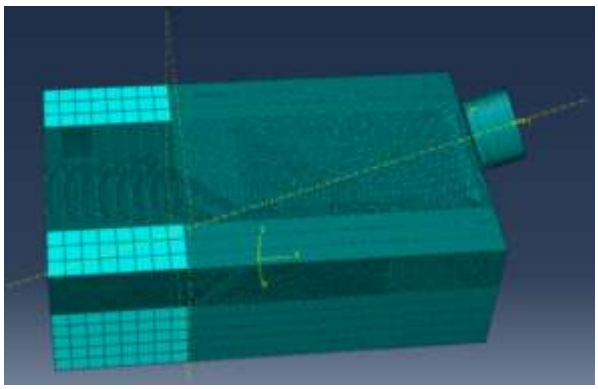

Fig. 4 Single tooth scraping finite element model

4. SIMULATION RESULTS AND ANALYSIS

In order to ensure the reliability of the single-tooth scraping rock simulation model, when the rock temperature is 300°C, the simulated cutting force is compared with the stable stage of the single-tooth scraping cutting force, as shown in Fig. 5. When the cutting teeth scrape the rock, the fluctuations in the load change reflect the volumetric fragmentation of the rock unit when being scraped. When the cutting teeth interact with the rock, the load on the cutting teeth will increase under the action of the reaction force. The load on the rock will continue to accumulate. When the load reaches the critical point of rock fragmentation, damage will occur, which will reduce the strength of the rock and reduce the load on the cutting teeth. After the rock crushing is removed, the cutting teeth are unloaded for a very short time, and the cutting force reaches the minimum. It is not until the contact with subsequent rock units begins that the cutting load continues to increase. Therefore, the cutting load fluctuates continuously when rock is broken. It can be seen that the overall trend of the simulation and experimental fluctuations is consistent. The average cutting load is 3412.3N, and the average cutting load of the simulation is 3226.6N. The error between the two is only 5.69%, thus verifying the reliability of the simulation model.

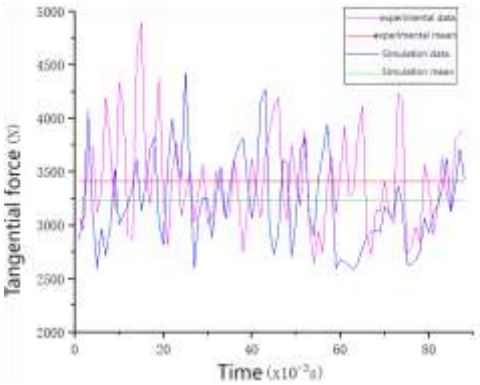

Fig. 5 Comparison of simulation and experimental cutting loads

4.1. Research on rock damage and tooth edge stress rules

4.1.1. Distribution pattern of rock damage degree

PEEQ equivalent plastic strain refers to the continuous accumulation of plastic strain under deformation conditions of the model. When the PEEQ value is positive, it indicates that the material in the model has yielded. Plastic strain is a permanent strain in material deformation, which can reflect the damage of the material to a certain extent. In order to effectively analyze the damage status of rocks at different temperatures, the same tiny unit is taken on the rock model, unit number 28913, as shown in Figure 6. The damage of this unit at different temperatures is shown in Fig. 6 As shown in Fig. 7 it can be seen from the damage results that as the temperature increases, the damage value of this unit first decreases and then increases, and the damage value is the smallest at 200°C. After exceeding 200°C, the damage value continues to increase, indicating that under certain conditions, high temperature can greatly reduce the strength of the rock, which is beneficial to the cutting teeth and greatly improves the rock breaking efficiency. This result shows that the cutting force first increases and then decreases, further explaining the crushing of rocks at high temperatures.

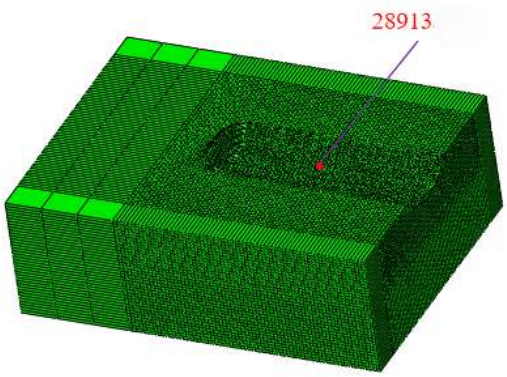

Fig. 6 Rock damage unit

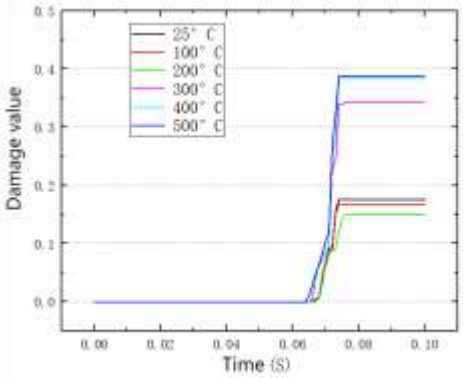

Fig. 7 Damage curves at different temperatures

4.1.2. Tooth edge stress distribution law

Fig. 8 shows the Cpress stress contours on the PDC cutter face when scraping rock at different temperatures. Stress only appears where the cutter touches the rock. The stress zone is mainly on the lower contact face and has a bow-shaped cross-section. As temperature rises, this bow-shaped zone becomes larger and the load on the cutter face more uniform. The maximum Cpress stress always lies just below the cutter edge tip—the zone that wears most easily—matching the wear pattern seen on field-used bits.

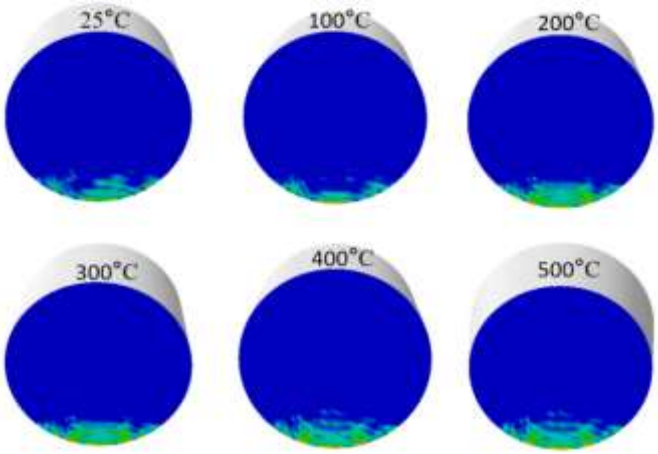

Fig. 8 Tooth surface contact stress cloud diagram at different temperatures

To analyze the Cpress stress on the cutter edge when it contacts the rock, the Cpress stress values at the element nodes along the edge from –90° to +90° were extracted. The lowest point of the cutter edge corresponds to a polar angle of 0°, as shown in Fig. 9.

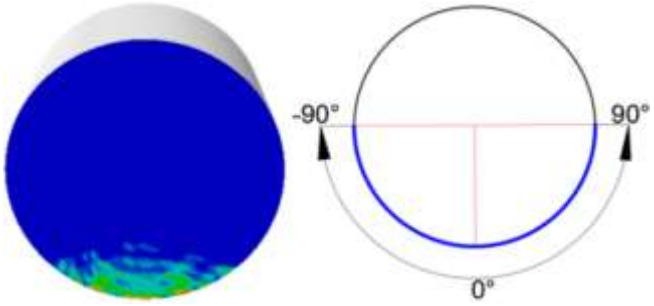

Fig. 9 Cutting tooth edge node area range

Fig. 10 shows the Cpress stress distribution on the cutter edge when cutting rock at different temperatures. From the figure:

- Stress rises from both sides of the edge toward the lowest point.

- The maximum Cpress stress appears near the lowest point and is symmetric there.

- The contact zone between edge and rock spans about 50°.

The highest Cpress stress occurs at ~200 °C, so the cutter experiences the largest load and wears fastest at this temperature. Above 200 °C, the stress drops as temperature increases.At ~200 °C the stress fluctuates most, giving a very uneven load on the cutter face and causing unbalanced wear; therefore this temperature is the least favorable for cutter life.

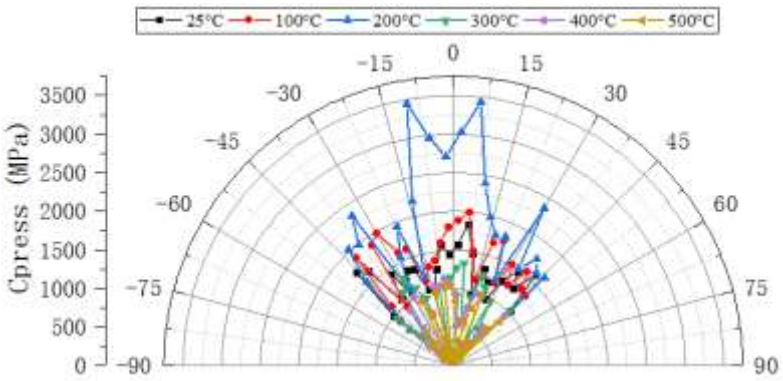

Fig. 10 Contact stress of tooth edge Cpress at different temperatures

4.2. Research on cutting tooth temperature field under different ambient temperatures

Fig. 11 shows the temperature distribution on the PDC cutter face when scraping rock at different temperatures. The hottest spot is not on the cutting edge, but a short distance away, forming a clear "hot band." Three reasons explain this:

1. Cutting produces many hot chips; these chips carry heat and land just behind the edge.

2. Temperature keeps rising during cutting; plastic deformation and friction near the edge accumulate heat.

3. At the set depth of cut, rock is compressed, and the work of deformation generates heat that flows into the cutter face.

Clear temperature-gradient layers appear from the cutter tip to the highest point and along the side in contact with the rock. The gradient decreases steadily away from the tip region until it reaches a stable value. This pattern arises because the temperature rise at the tip creates a temperature difference with the farthest regions of the face and side; heat is then conducted through the cutter, producing a smooth transition to equilibrium.

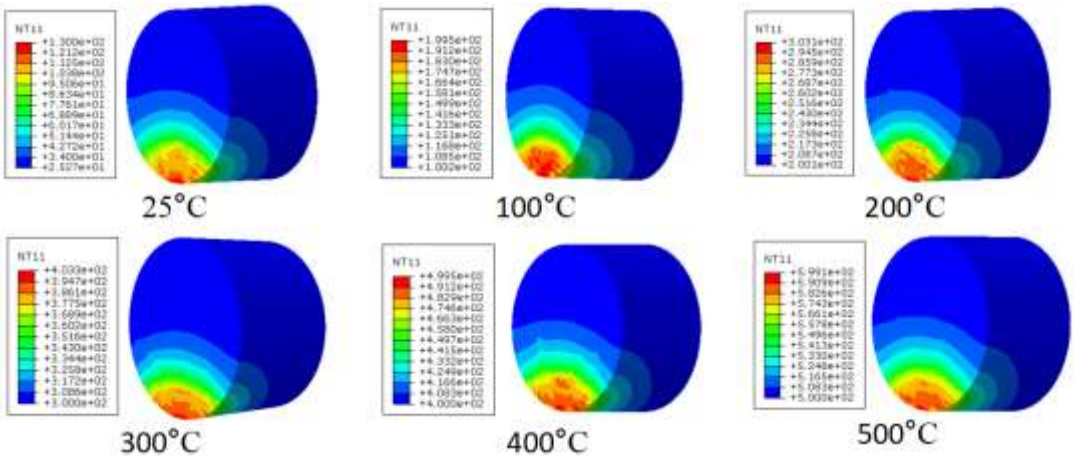

Fig. 11 Temperature field distribution of cutting tooth tooth surface at different temperatures (°C)

Fig. 12 shows the temperature contours on a single-cutter face at 300 °C for different scraping times. As cutting proceeds, the surface temperature rises, the color deepens, heat conduction becomes more evident, and the temperature gradient increases. The hottest zone remains near the cutting edge, where plastic deformation of the rock and chip–cutter friction concentrate heat; this concentration is the main cause of thermal wear and micro-cracking in high-temperature geothermal drilling.

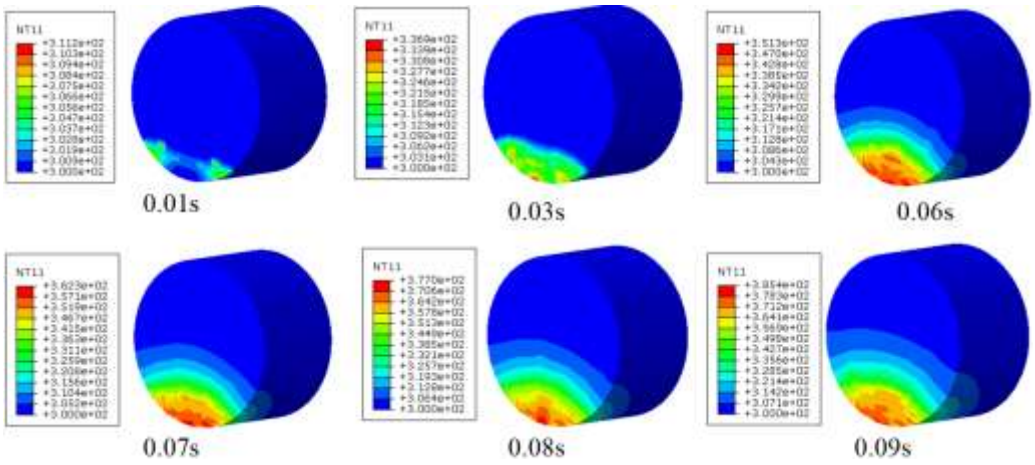

Fig. 12 Temperature field distribution of cutting tooth tooth surface at different times (°C)

At t = 0.04 s, nodal temperatures were extracted along the line defined by the cutting-edge tip diameter and the cutter axis on both the rake face and the flank. As the distance from the cutting edge increases, the face temperature first rises to a peak of 398.4 °C at 1.75 mm and then declines, stabilising beyond 7.55 mm. On the flank, temperature decreases monotonically from 390.7 °C at the edge, reaching steady values at about 7.05 mm.

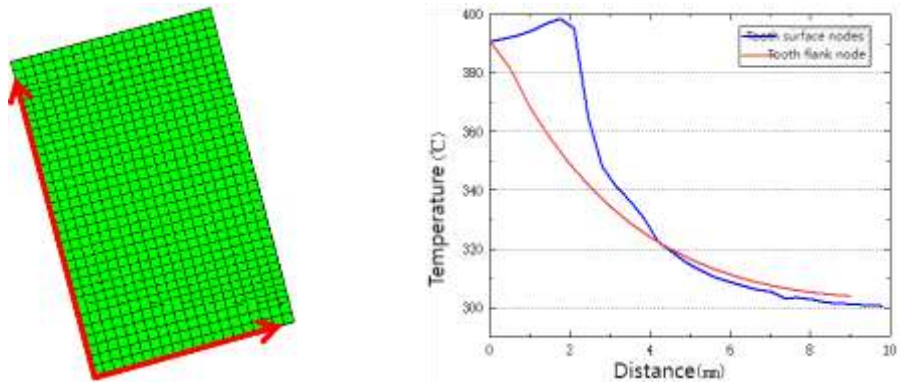

(a) Tooth front and side node distance (b) Relationship distance curve

Fig. 13 Tooth front and side node distance and distance curve

Fig. 14 presents the temperature evolution of selected rake-face nodes lying in the plane defined by the cutting-tip diameter and the cutter axis. During the initial rock engagement all nodes experience a rapid temperature rise; after a short cutting time the gradient flattens and the curves exhibit fluctuations consistent with the brittle–ductile nature of rock. Nodes located in or near the contact zone heat up faster, whereas remote nodes warm more slowly.

At first contact the rock is compressed and then fails under the combined effects of extrusion, shearing, friction and elastic–plastic deformation, generating a large amount of cutting heat. As scraping continues, this heat is shared between the cutter and the chips. Because the thermal conductivity of rock debris is much lower than that of the PDC, heat is conducted inward through the cutter while convective exchange at the chip–cutter interface returns part of the debris energy to the tool, producing the observed temperature history.

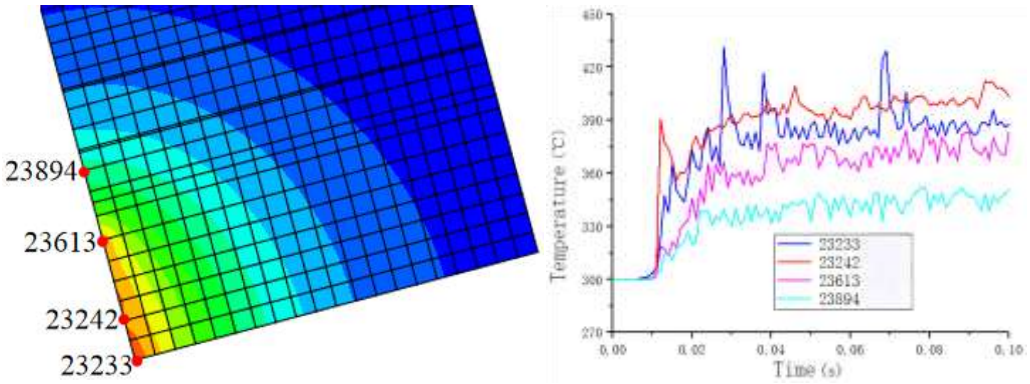

(a) Cutting tooth surface nodes (b) Temperature time curve

Fig. 14 Cutting tooth surface nodes and temperature time curve

4.3. Research on cutting tooth stress and temperature field under different cutting parameters

4.3.1. Distribution rules of cutting tooth stress and temperature field under different forward inclination angles

Temperature distributions on the cutter face at 300 °C for different rake angles are presented in Fig. 15. As the rake angle increases, the high-temperature zone expands and the hot region within the edge polar span becomes wider. Smaller rake angles produce a larger temperature-gradient area relative to the total face area, and the peak temperature is always located slightly behind the cutting-edge tip.

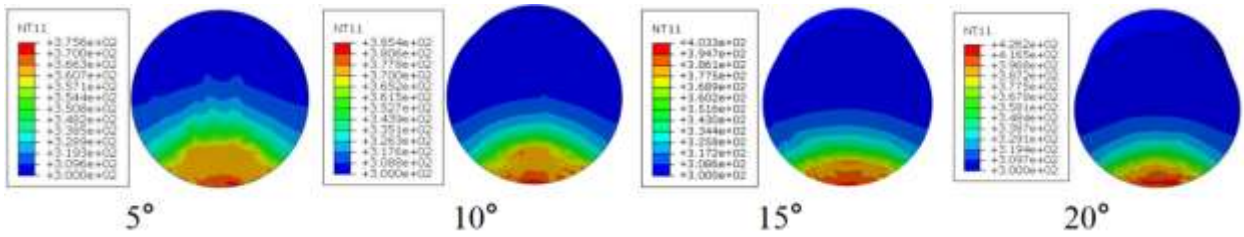

Fig. 15 Tooth surface temperature field at different forward inclination angles (℃)

Nodal-temperature profiles along the plane defined by the cutting-tip diameter and the cutter axis at a fixed instant are plotted in Fig. 16 for four rake angles. In every case the temperature first rises and then falls with distance from the edge, peaking at 1.75 mm, 1.05 mm, 1.75 mm and 2.1 mm behind the lowest cutting-edge point, with maximum values of 368.8 °C, 377.6 °C, 398.4 °C and 402.1 °C, respectively.

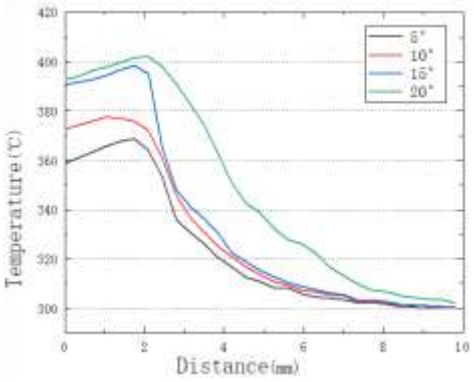

Fig. 16 Temperature curves of tooth surface nodes at different forward inclination angles

The Cpress stress distribution of the tooth edge when different forward inclination angles interact with rocks is shown in Fig. 17. It can be seen that as the forward inclination angle increases, the tooth

edge stress and stress fluctuation continue to increase. The main reason is that the greater the forward inclination angle, the greater the contact area with the rock, the greater the stress fluctuation on the tooth edge, and the stronger the squeezing effect of the cutting teeth on the rock, which is more likely to cause unbalanced wear of the cutting teeth and is less conducive to extending the working life of the cutting teeth. The Cpress stress is the largest near both sides of the lowest point of the tooth edge, and the contact area between the tooth edge and the rock for several forward inclination angles is 50°.

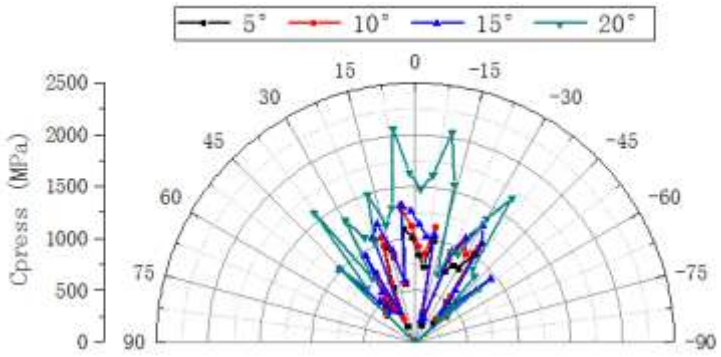

Fig. 17 Cpress stress distribution of tooth edge under different inclination angles

4.3.2. Distribution rules of stress and temperature field of cutting teeth under different cutting depths

The temperature distribution of the tooth surface when the cutting teeth interact with the rock under different penetration depths is shown in Fig. 18. It can be seen that as the penetration depth increases, the tooth surface temperature continues to increase. The main reason is that as the penetration depth increases, the contact area between the tooth surface and the rock continues to increase, and the cuttings scraped per unit time also increase. When the penetration depth is small, At that time, the cutting teeth mainly squeeze and break the cuttings. The increase in tooth surface temperature mainly comes from the heat conduction effect of the rock on the cutting teeth. When the cutting depth increases, the cutting teeth scrape the rock to produce a large number of fractured large cuttings. With the continuous scraping of the cutting teeth, the cuttings are continuously discharged and come into contact with the tooth surface, causing the tooth surface temperature to rise significantly. The deeper the rock is eaten, the more shear surfaces it encounters. The shear deformation of the rock increases, the work done increases greatly, and the heat generated by friction increases, which in turn causes the temperature of the cutting teeth to rise significantly. At 300°C, the maximum temperatures of the tooth surface at different depths are 378.2°C, 403.3°C, and 499.5°C respectively.

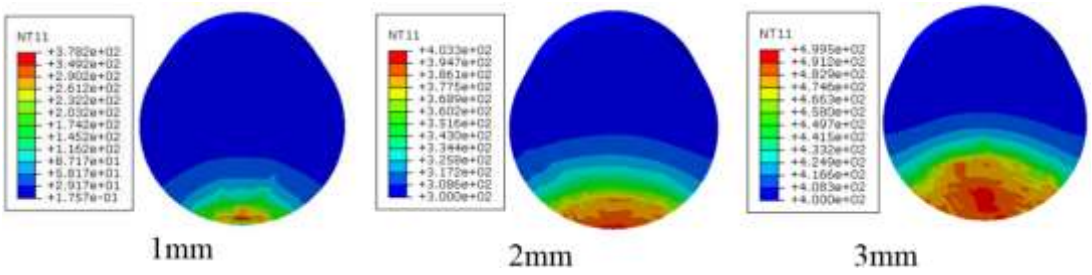

Fig. 18 Temperature field of tooth surface at different eating depths (°C)

The nodal-temperature profiles along the plane defined by the cutting-tip diameter and the cutter axis are plotted in Fig. 19 for three depths of cut. At every depth the temperature first rises and then falls with distance from the edge; the peaks occur at 0.7 mm, 1.75 mm and 1.05 mm behind the lowest point, respectively. A larger depth of cut gives a higher peak temperature, increasing the risk of thermal wear failure.

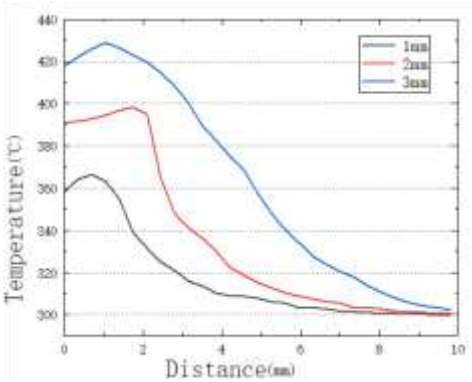

Fig. 19 Temperature curves of lower tooth surface nodes at different eating depths

The Cpress-stress distribution along the cutting edge for different depths of cut is displayed in Fig. 20. With increasing depth of cut the Cpress magnitude rises and remains symmetric about the edge tip. The contact arc expands from ≈ 30° at 1 mm depth to 50° at 2 mm and 58° at 3 mm. A larger depth enlarges the cutter–rock interface, lengthens the shear plane in the rock and raises the required cutting work. Deeper cuts also intensify stress oscillations, promoting uneven wear and shortening cutter life.

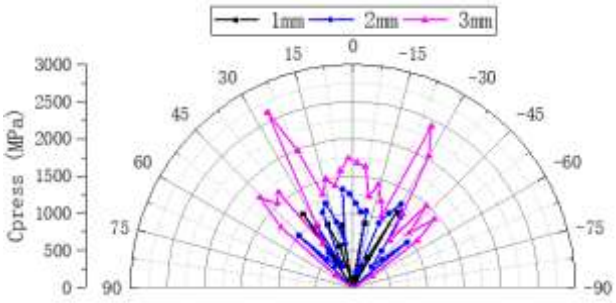

Fig. 20 Cpress stress distribution of lower tooth edge at different intake depths

4.4. Research on stress and temperature field of different tooth shapes under high temperature environment

PDC bits currently suffer from low penetration rates and poor rock-engagement capacity in geothermal drilling. To quantify the influence of cutter geometry, single-cutter scratching tests were performed at 300 °C under identical cutting conditions. The elliptical, roof-shaped and Mercedes-tip unconventional cutters illustrated in Fig. 21 were evaluated against a standard circular PDC cutter; resultant stress and temperature fields on each cutter face were compared.

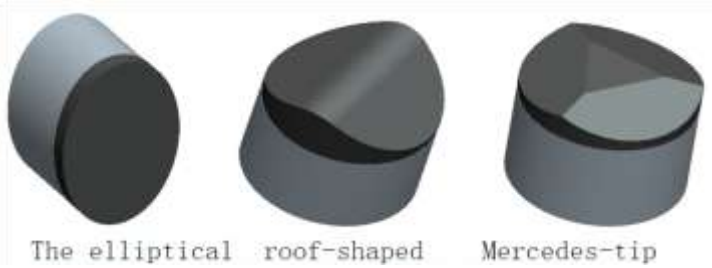

Fig. 21 Cutting teeth with different tooth surface shapes

Damage evolution of rock element No. 28913 during single-cutter scratching is displayed in Fig. 22. The Mercedes-tip and roof-shaped 3-D cutters trigger damage earliest, followed by the elliptical cutter, while the circular PDC is slowest. Peak damage values follow the same order: Mercedes-tip ≈ roof-shaped 3-D > elliptical > circular. These results confirm that 3-D cutters accelerate rock-strength degradation and improve fracture efficiency.

The superior performance of the roof-shaped and Mercedes-tip tools is attributed to “edge points” formed at the intersection of cylindrical flanks and ridge lines; these points indent the rock as sharp asperities, providing rapid penetration. In addition, the inclined side faces drag and pry the rock, further promoting fracture. The elliptical cutter, with its larger radius of curvature, presents a smaller contact patch than the circular PDC, generating higher tensile stresses and stronger upward lifting forces on the rock, and thus breaks rock more effectively than the conventional circular design.

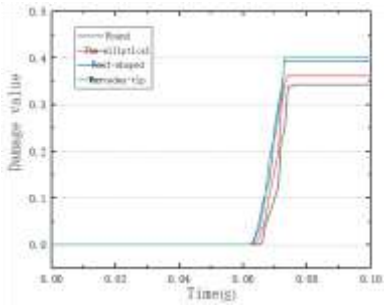

Fig. 22 Node damage curves under different tooth surface shapes

Cpress-stress contours on the cutting edge for different cutter geometries are given in Fig. 23. The circular PDC exhibits the highest Cpress stress, followed by the elliptical cutter, whereas the roof-shaped and Mercedes-tip 3-D cutters show the lowest values. Once rock is fractured and chips detach, contact is lost and the stress zone shrinks; this chip release governs the observed pattern. For the roof-shaped and Mercedes-tip cutters the peak stress appears on the ridge backs flanking the edge, where the “sharp-point” penetration squeezes and crushes the rock. All geometries display symmetric stress distributions about the lowermost point of the cutting edge.

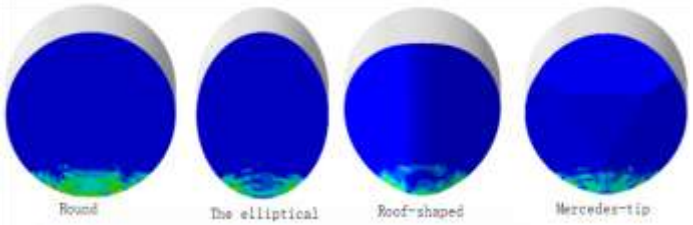

Fig. 23 Tooth edge Cpress stress cloud diagram under different tooth surface shapes

Cpress-stress distributions along the cutting edge for different cutter shapes are shown in Fig. 24. The circular PDC exhibits the highest Cpress stress, followed by the elliptical cutter, while the roof-shaped and Mercedes-tip 3-D cutters yield the lowest values. Compared with the circular PDC, the peak Cpress stress is reduced by 52.9 % for the Mercedes-tip, 52.4 % for the roof-shaped and 16.8 % for the elliptical cutter. The contact arc is 42° for both Mercedes-tip and roof-shaped cutters and 38° for the elliptical cutter. Lower stress fluctuations observed for the Mercedes-tip and roof-shaped designs indicate reduced uneven wear, which is beneficial for extending cutter life.

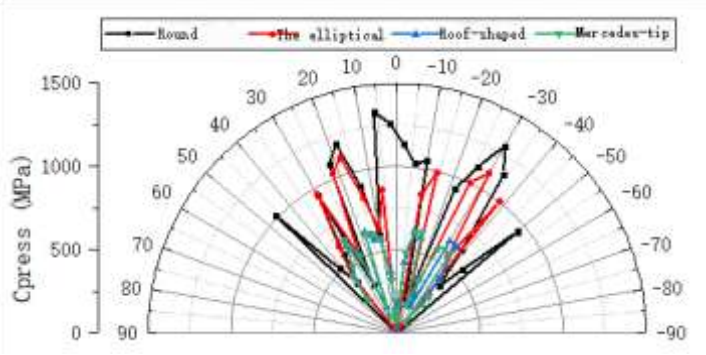

Fig. 24 Tooth edge Cpress stress distribution under different tooth surface shapes

Temperature distributions on the cutter face during single-cutter scratching are displayed in Fig. 25. The roof-shaped and Mercedes-tip 3-D cutters exhibit pronounced temperature-gradient fluctuations, whereas the circular and elliptical planar cutters show smooth, layered thermal fields. In the 3-D geometry, the ridge backs flanking the edge compress the rock and eject chips laterally; continuous chip generation and removal repeatedly bring hot debris into contact with the ridge-surface intersection, creating local temperature differences and strong thermal oscillations. Planar cutters conduct heat mainly through the edge, yielding gentler gradients. Compared with the conventional PDC, the high-temperature zones of the roof-shaped, Mercedes-tip and elliptical cutters are smaller; their peak face temperatures are 396.5 °C, 348.2 °C and 353.9 °C, respectively.

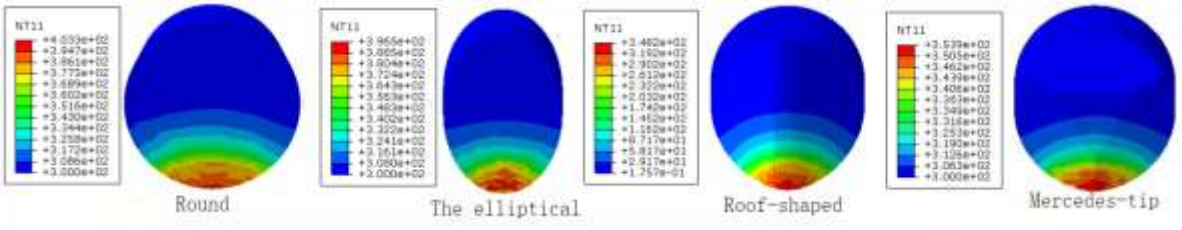

Fig. 25 Tooth surface temperature field under different tooth surface shapes (℃)

Nodal-temperature profiles along the plane defined by the cutting-tip diameter and the cutter axis at the same instant are plotted in Fig. 26. For every cutter shape the temperature first rises and then falls with distance from the edge. The circular cutter produces the highest nodal temperature, followed by the elliptical cutter, while the Mercedes-tip and roof-shaped 3-D cutters yield the lowest values. Peak temperatures—398.4 °C, 360.7 °C, 340.1 °C and 345.1 °C—occur at 1.75 mm, 1.05 mm, 0.35 mm and 0.35 mm behind the lowest cutting-edge point, respectively.

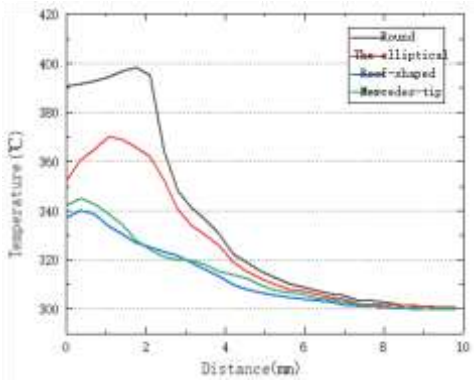

Fig. 26 Tooth surface node temperature curves under different tooth surface shapes

In summary, three-dimensional cutters such as roof-shaped and Mercedes-tip inserts induce greater rock damage, achieve higher fracture efficiency and exhibit lower stress-wave amplitude under hard, highly abrasive and high-temperature down-hole conditions; these characteristics prolong cutter life and make the 3-D geometries better suited for high-temperature geothermal drilling.

5. CONCLUSION

By simulating particle-scale fragmentation at elevated temperatures, this paper quantifies how cutting forces vary with depth of cut, rake angle and cutter geometry while scraping rock at different temperatures. Systematic numerical experiments further map the resulting stress and temperature fields on the cutter face under each parameter combination. The derived load and thermal characteristics provide a theoretical basis for the optimised design of drill bits aimed at high-temperature geothermal applications.

(1) Single-cutter scratching simulations were run at various rock temperatures. The maximum tensile stress and the peak Cpress stress on the cutting edge both occur at 200 °C. The hottest zone on the cutter face is located slightly behind the edge, forming a distinct “hot band”.

(2) Parametric studies show that increasing depth of cut raises both the face temperature and the edge Cpress stress. A larger rake angle produces higher Cpress stress and a hotter cutter surface.

(3) Three-dimensional cutters (roof-shaped and Mercedes-tip) generate greater rock damage and higher fracture efficiency under high temperature, delay delamination and abrasive failure, and thus extend cutter life. Worn cutters were also examined: after wear the cutting load rises by 74.2 %–173.9 %, the specific cutting energy increases by 26.5 %–71.7 %, and the peak temperature climbs sharply. These results indicate that once wear initiates in geothermal drilling, the resulting temperature surge accelerates thermal damage and rapidly shortens cutter life.

REFERENCES

[1] Shulyupin A N. Steam-water flow instability in geothermal wells [J]. Thermophysics and Aeromechanics, 2015, 22 (4):475-480.

[2] Zha Yongjin, Feng Xiaowei, Ge Yunhua, Chen Zhixue. Progress in high-temperature geothermal power drilling technology [J]. Science and Technology Herald, 2012, (32):51-54.

[3] Gioia Falcone. Oil and Gas Expertise for Geothermal Exploitation: The Need for Technology Transfer [C]. SPE 113852, 2008.

[4] Bi Yurong. Review of current status and prospects of geothermal resource development and application[J]. Petroleum and petrochemical energy conservation, 2011, (10): 7-11.

[5] Li Jifei. Simulation research and performance analysis of hot dry rock power generation technology[J]. Shandong Chemical Industry,2021,50(09):114-119.

[6] Zhang Jie, Zhao Meng, Niu Shiwei. Progress and development trends of key technologies for hot dry rock EGS [J]. District heating, 2021(02): 79-84.

[7] Hu Shukai, Tian Feng, Li Hanyue, et al. Development and application of high-efficiency wear-resistant PDC drill bits for ultra-high temperature geothermal drilling [J]. Drilling and Production Technology, 2020, 43(03): 1-3+141.

[8] Lukawski M Z, Silverman R L, Tester J W. Uncertainty analysis of geothermal well drilling and completion costs [J]. Geothermics, 2016, 64: 382-391.

[9] Frolova J V,Ladygin V M, Rychagov S N. Petrophysical alteration of volcanic rocks in hydrothermal systems of the kuril-kamchatla Island Arc[C]. World Geothermal Conpress, 2010.

[10] Greg Bignall. Taupo volcanic zone deep geothermal drilling project [EB/OL]. http://www.gns.cri.nz/ content/download/6786/37092/file/2-3_HADES_May2011_Bignall_GNS-Science.pdf

[11] Guang Xinjun, Wang Minsheng, Sina, et al. Difficulties and countermeasures in high-temperature geothermal high-efficiency development drilling technology [C]. Proceedings of the 18th National Exploration Engineering (Geotechnical Drilling Engineering) Technology Academic Exchange Annual Conference. Harbin, Heilongjiang, China. 2015.

[12] Zuo Ruqiang. Overview of the progress of international oil and gas well drill bits (Part 3) - PDC drill bit development process and current situation (Part 1) [J]. Exploration Engineering, 2016, 43(3): 1-8

[13] Zuo Ruqiang. Overview of the progress of international oil and gas well drill bits (4) - PDC drill bit development process and current situation (Part 2) [J]. Exploration Engineering (Geotechnical Drilling Engineering), 2016(04): 40-48.

[14] Scott DAN. A bit of history: Overcoming early setbacks, PDC bits now drill 90%-plus of worldwide footage[J]. Drilling Contractor anthology series—PDC drilling bits. Houston, TX: IADC, 2015: 1-7.

[15] Andersen E E, Azar J J. PDC Bit Performance Under Simulated Borehole Conditions[J]. Drilling & Completion, 1993, 8: 184-188.

[16] Zhu Lihong, Chen Zepeng, Huang Yong, Qiang Wei, Wang Jingyin. Experimental study on the anti-adhesion performance of the non-smooth surface of the PDC drill bit body[J]. Laboratory research and exploration, 2018, 37(10): 27-30.

[17] Robert H Frushour, Devonshire, Ann Arbor. Composite polycrystalline diamond compact with improved impact and thermal stability [P], USA: United States Patent 5645617,1997.